Quantum-Dot-Tagged Reduced Graphene Oxide Nanocomposites for Bright Fluorescence Bioimaging and Photothermal Therapy Monitored In Situ

*Shang-Hsiu Hu, Yu-Wei Chen, Wen-Ting Hung, I-Wei Chen, and San-Yuan Chen**

Nanomedicine demands nanocarriers that combine multiple functionalities, such as imaging, drug delivery and photothermal therapy, into a single system. Various functional nanoparticles (e.g., semiconductor quantum dots (QDs), gold nanoparticles, magnetic nanoparticles, carbon nanotubes, and graphene nanosheets) have found applications in ultrasensitive diagnosis, imaging and therapy.[1–6] However, further innovations to dramatically improve their current capabilities are still needed for practicable nanomedicine. For example, without the ability of bright imaging and precise monitoring of therapeutic progress, hyperthermia treatments can leave unintended damage or side effects to healthy organs and tissues. Nanocomposites capable of imaging and therapeutic and in situ monitoring modalities may offer solutions to these issues; they are also of interest in molecular imaging and biosensing.

Compared with traditional fluorescent molecules, QDs have brighter fluorescence, narrower photoluminescence spectra, lower photoleaching and more resistance to chemical degradation.[7] However, they also exhibit a higher toxicity[8] and lack therapeutic functions.[9] Therefore, it would be desirable to: a) re-engineer QDs to reduce their toxicity while preserving their fluorescent property, and b) supplement them with an optically active therapeutic agent, such as a photothermal-therapy agent that converts absorbed light into local heating, for cell killing in a minimally invasive manner. Such photothermal therapy prefers near-IR (NIR) radiation, which has deep-tissue penetration with minimal normal tissue damage, even at high spatial concentrations.[10] Several NIR-absorbing photothermal nanoparticle agents, such as gold nanorods,[11] carbon nanotubes[12] and graphene nanosheets,[13] which are administered in a site-specific manner, have been developed to provide local heating and treatment of diseased regions. Along this line, graphene oxide nanosheets that have a large surface area and a strong NIR absorbance are also a potential NIR photothermal agent, as already illustrated by in vivo experiments.[14,15] Indeed, since graphene oxide nanosheets are not strongly fluorescent, their combination with QDs would seem complementary. In addition, Sun and coworkers have reported that graphene nanosheets with covalently attached polyethylene glycol (PEG) polymer chains can passively accumulate in tumor vasculatures and thus may potentially serve as a carrier for drug delivery.[16,17] However, although QDs can be tethered to graphene oxide,[18] this approach of direct conjugation of QDs to graphene oxide has, so far, failed because the QD fluorescence in the conjugated nanocomposite becomes nearly completely quenched due to energy transfer from the QDs to the graphene.[19,20]

In this work, we report a novel, strongly fluorescent, non-toxic QD-tagged reduced graphene oxide (QD-rGO) nanocomposite that combines the capability of cell/tumor bioimaging with photothermal therapy, as demonstrated in vitro and in vivo. This nanocomposite has overcome several of the obstacles mentioned above: the QD toxicity is mitigated by a surfactant coating, and the fluorescence quenching is greatly reduced by maintaining a precisely controlled spacer between the QDs and the rGO. Remarkably, as the QD-rGO absorbs NIR irradiation, to cause photothermal therapy and cell killing, the generated heat from the QD-rGO simultaneously causes a temperature increase and a marked decrease in the QD brightness, which provides a means for in situ heat/temperature sensing and an indicator of the progress of the photothermal therapy. Meanwhile, active targeting and enhanced cell internalization through the conjugation of the QD-rGO with targeting/internalization ligands has also been achieved. The integration of these functionalities makes this nanocomposite a potentially viable new tool for cancer diagnosis, imaging and treatment through both drug/molecule delivery and photothermal therapy.

Graphene oxide sheets (GSs) were synthesized from graphite using a modified Humme's method.[21] The resulting GSs were easily sedimented in aqueous solution with a mean size of about 2.5 μm, measured by dynamic light scattering (DLS) (**Figure 1**a). After centrifugation at 12 000 and 20 000 rpm, suspensions of two GS sizes, 38 and 260 nm, respectively, were obtained (Figure 1a).[16] To reduce the GSs to rGO, hydrazine monohydrate was added to the solution and the mixture was heated to 80 °C. The QDs used were initially protected by a high-density coating of tri-n-octylphosphine oxide (TOPO), a standard treatment to achieve strong fluorescence. As illustrated schematically in Figure 1b, when TOPO is partially substituted by 11-mercaptoundecanoic acid (MUA), a monolayer organic shell of a well-defined thickness was formed on the QD surfaces. This became apparent by examination of the self-assembled QD aggregates, each of which formed a face-centered-cubic (fcc) array of QDs[22–24] with a lattice parameter of 7.4 nm and a closest QD spacing of 5.36 nm (see Figure S1); this is clearly

Dr. S.-H. Hu, Y.-W. Chen, W.-T. Hung, Prof. S.-Y. Chen
Department of Materials Sciences and Engineering
National Chiao Tung University
Hsinchu, 300, Taiwan
E-mail: sanyuanchen@mail.nctu.edu.tw
Prof. I.-W. Chen
Department of Materials Sciences and Engineering
University of Pennsylvania
Philadelphia, PA 19104-6272, USA

DOI: 10.1002/adma.201104070

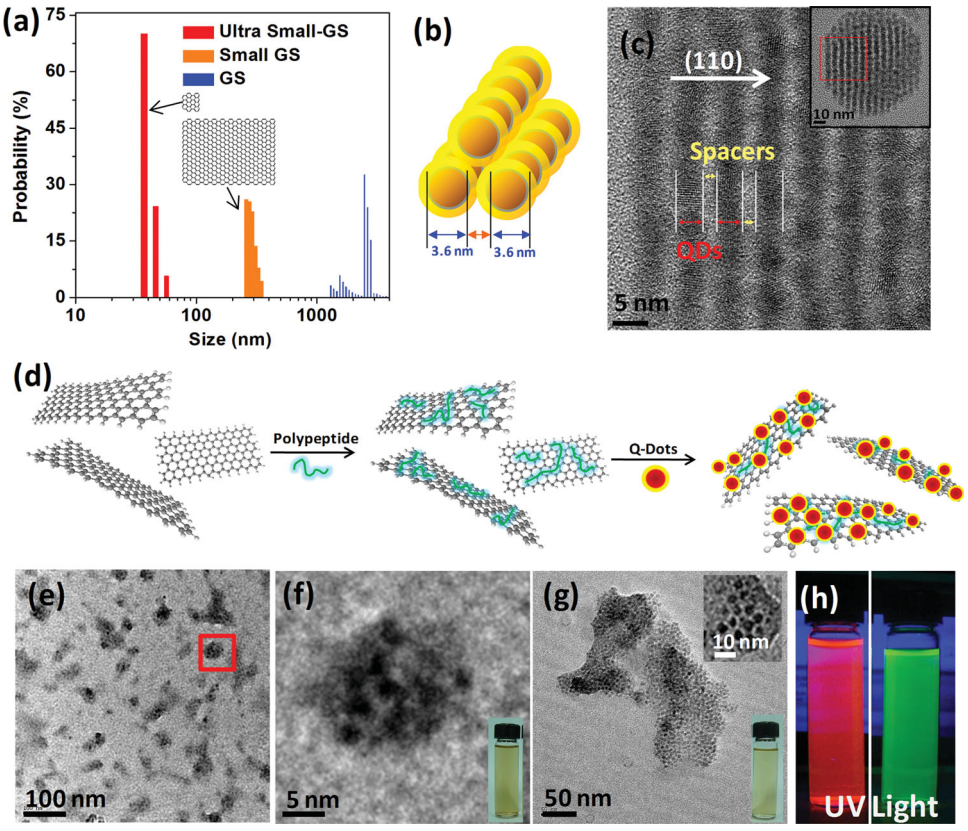

Figure 1. a) Size distributions of ultra-small graphene nanosheets (GSs), small GSs, and as-prepared GSs, measured by dynamic light scattering. b) Schematic illustration of coated QDs in (fcc) self-assembly. c) High-resolution TEM image of the self-assembly structure in Figure 1b, showing the 110 "lattice fringes" of the fcc QD array with a gap of 1.7 nm between the QDs due to the coating; inset: at a lower magnification. d) Schematic showing poly (L-lysine) adsorption onto rGO, allowing subsequent QD adsorption/conjugation. e) TEM image of the QD-tagged 38 nm rGO. f) Higher-resolution image of the area shown in Figure 1e. g) TEM image of the QD-tagged 260 nm rGO. A higher-resolution image of an area in Figure 1g is shown in the upper right inset. The insets at the lower right of Figure 1f and 1g show the sample suspensions under visible light. h) Suspensions of two QD-rGO samples under UV light.

shown in Figure 1c by the "110-lattice fringe imaging"[22] of the fcc QD array oriented in the 001 zone axis, under transmission electron microscopy (TEM). These figures and their enlargement (e.g., Figure) show a well-ordered particle (3.6 nm) array separated by gaps of 1.7 nm, which may be attributed to the organic coating.

To attach QDs to the rGO, as shown in Figure 1d, we first modified the rGO by the surface adsorption of an amphiphilic polypeptide, poly(L-lysine), which is shorter than serine proteins, but has similar functions, such as improving dispersion and endowing good adhesiveness to the rGO surface.[25,26] During overnight incubation at room temperature, QDs were adsorbed to the polypeptide-rGO of both the 38 nm (denoted as ultra-small rGO (US-rGO)) and 260 nm rGO (denoted as small rGO (S-rGO)) at high densities, forming QD-rGO nanocomposites (Figure 1e and 1g). The high-resolution TEM (HR-TEM) images shown in Figure 1f and in the inset of Figure 1g confirm that the QDs were actually separate from each other and formed a quasi-regular 2D array with apparently good interface adhesion (i.e., no visible cracks). This suggests that the TOPO and MUA surfactants were effective in maintaining a gap between the QDs, and presumably between the QDs and the rGO, which is important for reducing fluorescence quenching. Fluorescence is verified in Figure 1h, which shows two UV-illuminated suspensions containing QD-US-rGO made of two-sized (colored) QDs. The dramatic improvement against quenching was found to be the direct result of using MUA as a spacer (estimated length ≈ 1.8 nm): a similar, but shorter, mercaptopropionic acid (MPA) spacer (estimated length ≈ 0.7 nm) was less effective in reducing quenching (Figure S2). In addition to the color, the density of the QDs on the rGO could be controlled by changing the QD concentration in solution (Figure S3, Supporting Information). These QD-rGO samples were highly stable: they showed only a minimal fluorescence loss after 24 h of ambient storage in phosphate buffered saline (PBS). (Figure S4, Supporting Information).

The photoluminescence (PL) response of the QD-rGO was found to depend strongly on the size of the rGO. At the same molar concentration of QDs (3.4×10^{-4} mmol) and independent of the wavelength of the excitation/emission used, the fluorescence of the QDs supported on the US-rGO was lower than that of free QDs by 15%, and the fluorescence of QDs on the S-rGO was lower by 50% (**Figure 2**a,b). To further confirm the "size" effect, which was on intensity and not on wavelength, we also tested QDs supported on micrometer-sized rGO, and found essentially no fluorescent signal. The above results have

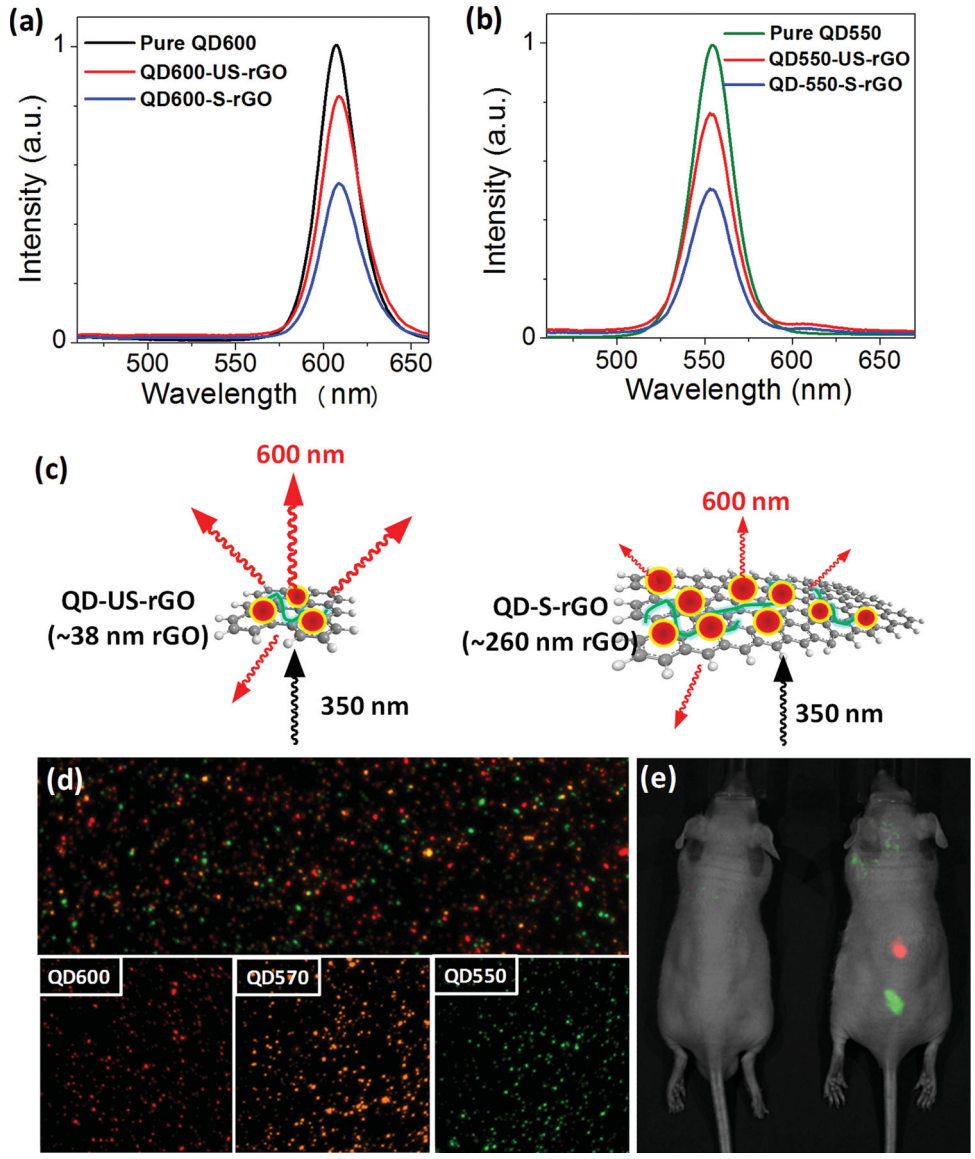

Figure 2. a,b) Fluorescence spectra of free QDs (two sizes), QD-S-rGO and QD-US-rGO emitting at 600 nm (a), and 550 nm (b). c) Schematic of shielding effect of rGO for the two sizes, absorbing more incoming irradiation (350 nm, from below) and stimulating less QD fluorescence (above, 600 nm) by the larger rGO. d) Multicolor fluorescence image of a mixture of three QD-rGO samples (with QD emissions at 550, 570 and 600 nm) spread onto a glass slide. e) Mouse before and after injection of two QD-rGO solutions (with QD emissions at 550 and 600 nm).

nothing to do with quenching, since all of the QDs had the same surface coating, which should have reduced the quenching; moreover, the spacing between the QDs was not correlated to the rGO size according to TEM. Instead, it may be attributed to the radiation-shielding effect[27] of a conductor, such as the rGO, which increases with latter's size. This is especially effective since rGO is known to be a good light-absorber.[11] This "size" effect is schematically indicated in Figure 2c. Fortunately, the size effect does not affect the ability of obtaining a multicolored spectrum using different-colored QDs on rGO because the shielding effect is apparently wavelength independent. This is illustrated in Figure 2d, which shows a multicolor fluorescent image from a glass slide that contained a spread mixture of three differently colored QD-US-rGO samples under irradiation from a single UV source. To demonstrate that the PL may be used for in vivo imaging of internal tissues in small animals, we injected, through subcutaneous injection (≈2 mm deep), two sets of QD-US-rGO (100 μL each) – one tagged with green QDs, the other with red QDs – into a nude mouse at two locations, using a procedure similar to that reported by Han et al.[28] As shown in Figure 2e, two fluorescently colored regions in the mouse were clearly visible.

For effective drug delivery and photothermal therapy, it is desirable that the nanoparticle carrier can enter the target cell. The folate mechanism provides one uptake mechanism, through folate-receptor (FR)-mediated endocytosis, which first internalizes a folic acid (FA) molecule captured by an FR, then returns the FR to the cell surface to capture more FA (FR and FA have

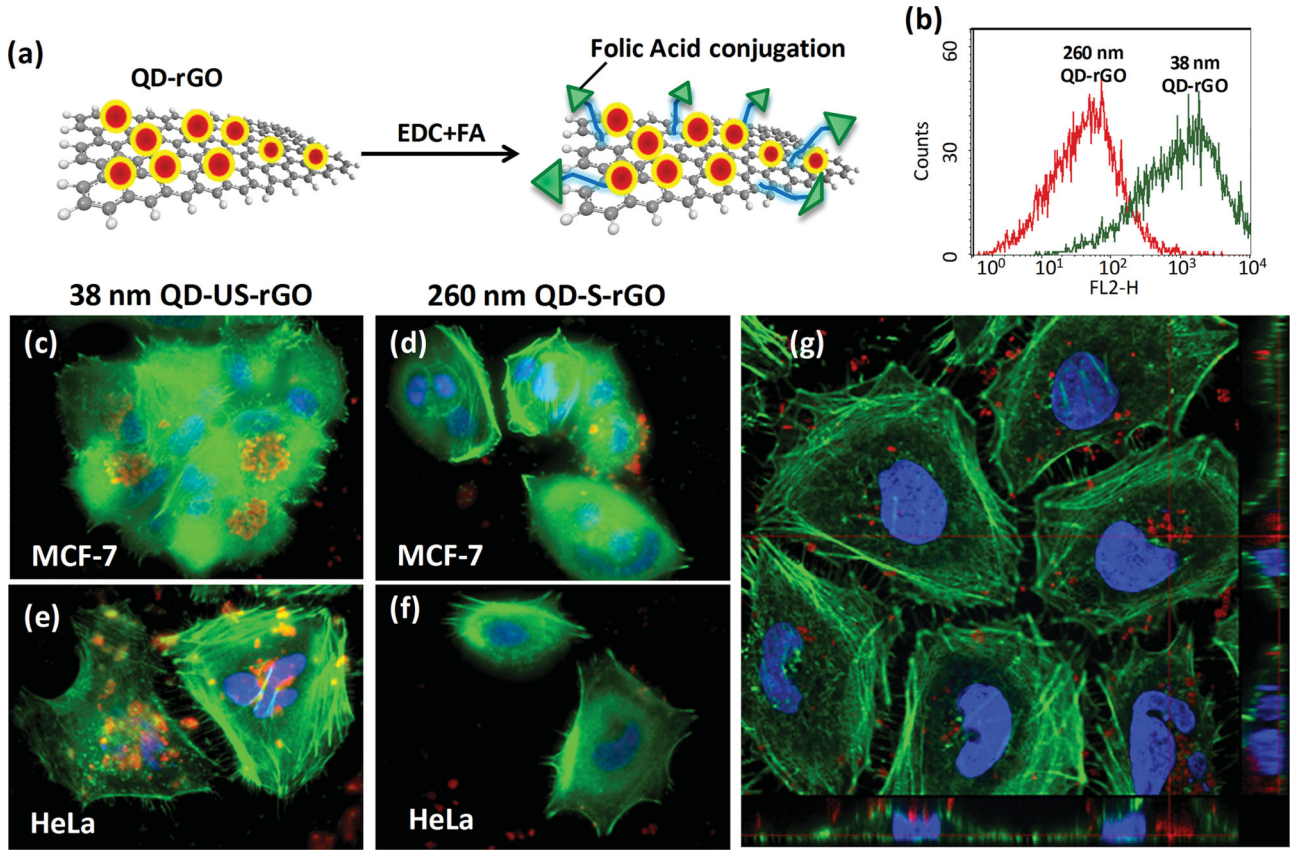

Figure 3. a) The QD-rGO (left) and the folic acid (FA) conjugation to the QD-rGO (right). b) Flow-cytometry analysis of the QD-US-rGO (260 nm) and the QD-S-rGO (38 nm) in MCF-7 cells after incubation for 6 h. c–f) Cellular uptake of FA-QD-US-rGO in MCF-7 cells (c) and HeLa cells (e) showing QD fluorescence (red-orange) in many regions, including the blue ones (cytoplasm), and that of FA-QD-S-rGO in MCF-7 cells (d) and HeLa cells (f), showing QDs mostly at the cell surfaces. g) Confocal images of multiple cross-sections, exhibiting various locations of the QD-rGO within the cells.

very-strong binding). This mechanism also operates when FA is tethered to a nanoparticle,[29] thus providing an internalization mechanism for the latter, which may be used for targeted tumor imaging and treatment (FR is overexpressed in many tumor cells, including ovarian, lung, kidney, colon, prostate and throat tumors, but not in normal cells[30]). To demonstrate the internalization of the QD-rGO, we first covalently tethered FA onto the surface of the QD-rGO via the linkers provided by poly(L-lysine) (**Figure 3**a). Flow cytometry was then used to verify the binding of FA-QD-rGO with FR-expressing MCF-7 cells. This is demonstrated in Figure 3b, which shows the fluorescence spectra of flow cytometry after the nanocomposites were incubated with Michigan Cancer Foundation 7 (MCF-7) cells for 6 h. Although both the QD-US-rGO (38 nm) and the QD-S-rGO (260 nm) cells showed fluorescence, the fluorescence intensity (the horizontal axis) from the former was about 20 times stronger, which was much higher than expected from the size effect (Figure 2a,b) alone. This suggests more binding or uptake of the QD-US-rGO to the cells. Fluorescence microscopy of MCF-7 cells incubated for 24 h showed most of the QD-S-rGO remained at the cell surface (Figure 3d), but the QD-US-rGO could be observed in the cytoplasm (Figure 3c). These observations were also confirmed in another FR-expressing cell line, Henrietta Lacks (HeLa) cells, shown in Figure 3e (QD-US-rGO) and Figure 3f (QD-S-rGO). Moreover, the bright QD-US-rGO appeared to be localized as discrete dots, suggesting no QD leaching from the nanocomposites. The cross-sectional confocal images in Figure 3g for the MCF-7 cells incubated with the QD-US-rGO also verified that many regions of the cytoplasm contained these nanoparticles, a further confirmation of their effective internalization. The size effect on the cellular uptake of nanomaterials has been documented in other systems.[31,32] In our study, 38 nm clearly lies below the size threshold for enhanced uptake. Control experiments of cells incubated without QD-rGO (Figure S5) confirmed that the red-orange color in Figure 3c–g was due to the QDs.

Having demonstrated the nanoparticle internalization, we were in a position to evaluate the toxicity and photothermal therapy of the QD-US-rGO. The 3-(4,5-dimethyldiazol-2-yl)-2,5 diphenyl tetrazolium bromide (MTT) assay, which measures the metabolic activity of cells, was used to evaluate the cytotoxicity of QD-rGO in incubated HeLa and MCF-7 cells. The results (Figure S6) revealed negligible differences in cell viability over an incubation period of 12 to 48 h with or without nanoparticles. At the highest concentration of 20 mg L^{-1} QD-rGO, the cell viability remained at approximately 92%. In contrast, the "free" MUA-QDs and MPA-QDs (not tethered to rGO) caused lower cell viabilities of 75% and 65%, respectively. Thus the colocation of the QDs and rGO, as well as a more-robust protective coating, apparently mitigates the toxicity.

To evaluate the photothermal therapy, we irradiated MCF-7 cells administered with QD-US-rGO (red QDs in 20 mg cm^{-1}, in terms of the rGO amount, incubated for 24 h) at a NIR wavelength of 808 nm and 2 W cm^{-2} for 4 min (see schematic in **Figure 4**a). After irradiation, the cells were stained with propidium iodide to characterize the cell viability: live cells appear in green. Before irradiation, live cells (green) and fluorescent QDs (red) were both highly visible in the entire region, as shown in Figure 4b. After irradiation, the region irradiated – its boundary marked by the white dashed line in Figure 4b – had almost no live cells or red-colored QDs left, indicating that the irradiation had killed almost all of the cells and simultaneously caused the loss of QD fluorescence. The loss of fluorescence due to irradiation was further investigated by subjecting a water suspension of QD-rGO, without cells, to the same laser irradiation at the same power for different durations: indeed, the intensity of the PL emission at 600 nm decreased with irradiation time (Figure S7a, Supporting Information). This loss of fluorescence proved irreversible: after irradiation was discontinued, no recovery was seen, even after a long waiting time. Meanwhile, the same experiment (in a solution of 5 mL) found a rapid increase in temperature with irradiation time, reaching 67 °C in 5 min due to the heat generated from the QD-rGO (Figure S7b). Parallel experiments found the same heating effect in solutions containing only rGO without QDs; however, solutions containing only QDs without rGO had no discernable heating (Figure S8). These results show that the heating effect was entirely due to the rGO, which is consistent with observations by Robinson and coworkers who reported that rGO displays a 6-fold higher NIR absorption than nonreduced GO.[11] Also consistent with the above observations, we found no fluorescence degradation for the QDs when the rGO was absent (Figure S8b, Supporting Information). Furthermore, another set of control experiments for cells irradiated without QD-rGO found no cell damage under laser irradiation (Figure S9, Supporting Information). Therefore, we may conclude that the rGO was responsible for the photothermal heating, which caused both the cell killing and the QD fluorescence degradation. The latter is likely to be due to the destruction of the TOPO/MUA coating (see below), and may be used provisionally as a measure of temperature or thermal dosage.

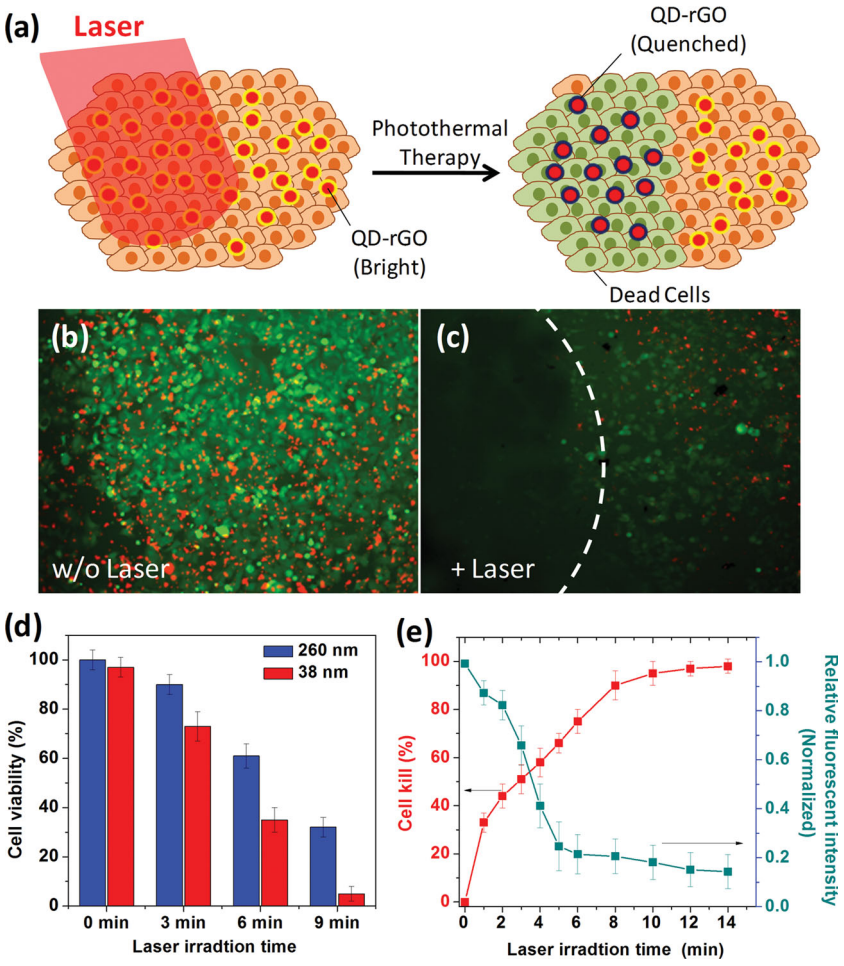

Figure 4. a) Schematic illustration of QD-rGO under irradiation (left) causing cell death and diminished QD fluorescence (right). b) Before irradiation, the cells incubated with the FA-QD-US-rGO were viable (green) and the internalized QDs were fluorescent (red). The live cells were stained with propidium to appear in green. c) After irradiation (808 nm for 4 min, in region left of the marker curve), essentially all of the cells were killed and the fluorescence was absent. d) The viability of cells incubated with FA-QD-US-rGO (38 nm) and FA-QD-S-rGO (260 nm) versus the duration of the irradiation. e) Cell death and normalized fluorescence intensity for cells incubated with FA-QD-US-rGO after irradiation for various durations.

Figure 4d exhibits the cell viability of the MCF-7 cells incubated with the QD-rGO under different irradiations. Prior to irradiation, the cells were incubated for 8 h with FA-conjugated QD-rGO. After 9 min of irradiation, the cell viability decreased to less than 5% when QD-US-rGO was used. This compares with more than 30% when using QD-S-rGO. Therefore, although the same overall heating was provided by the rGO (Figure S7b), which could obviously cause cell death over time, a faster cell killing was achieved when the rGO was delivered into the cytoplasm (Figure 3c and 3e), providing concentrated heating inside the cells. We also used FA-rGO, without QDs, and verified that it also produced the same low cell viability as FA-QD-rGO. This confirmed that the fast cell killing was caused mainly by the rGO delivered into the cytoplasm and not by the QDs. Importantly, the cell viability shows a one-to-one correlation with the QD fluorescence intensity in Figure 4e. This indicates that the progress of photothermal therapy can be monitored precisely and estimated quantitatively, optically, using the QD fluorescence intensity.

Lastly, we briefly discuss a possible mechanism for the fluorescence degradation during heating. It is clear that there was a substantial temperature rise (Figure S8a) due to the optical

absorbance of the rGO. The actual local temperature rise at the rGO heat source affecting the QDs on the QD-US-rGO directly should be even higher, since the measured temperature rise was only a "mean-field" value, averaged over the environment after the heat generated was shared by both the rGO and the surroundings (mostly water). Although TOPO is known to be highly heat resistant, MUA is likely to degrade under excessive heat, causing the deterioration of the coating and the loss of the protection of the QDs. Subsequent oxidation could then lead to the loss of fluorescence.[33] This was supported by the following experiment): a water suspension of QD-rGO was found to suffer from progressive fluorescence degradation as the water temperature rose, indicating that it was heat, not irradiation, that caused damage to the MUA-coated QDs. To provide further support for this mechanism, we investigated another "model" QD, CdSe/ZnS, tagged to the rGO, again subject to laser irradiation. The X-ray-photoelectron-spectroscopy (XPS) analysis (Figure S10, Supporting Information) indicated a rapid oxidation of the ZnS after a short time, which could also occur to the TOPO/MUA-coated QDs when supported on a laser-heated rGO substrate.

In summary, a novel, multifunctional, low-toxicity QD-rGO nanocomposite has been developed to serve as an imaging agent in the visible-light region and a photothermal cancer-therapy agent in the NIR region. These results were made possible by the use of a suitable nanosized spacer that separated the QDs and the rGO, thereby reducing fluorescent quenching. Meanwhile, since the thermal effect of the irradiated rGO could cause not only cell killing, but also the degradation of the QDs, the QDs also served as an optical indicator for the heat dosage and the therapeutic progress. These effects were most evident when the QD-rGO was guided by a targeting moiety, such as folate, that delivered the nanocomposite into the cytoplasm. Such nanoplatforms with built-in capabilities for in situ imaging, treatment and monitoring are expected to open a new avenue for radiation therapy in general, possibly leading to clinical applications.

Experimental Section

Poly(L-lysine)-rGO Conjugation: In a typical process, 1 mL of an aqueous solution containing rGO (20 mg mL^{-1}) and poly(L-lysine) (20 mg mL^{-1}, polypeptide, Sigma–Aldrich) were incubated in 2-amino-2-hydroxymethyl-propane-1,3-diol (Tris)/boric acid/ethylenediaminetetraacetic acid (EDTA) (TBE) buffer (Tris, 44.5×10^{-3} M; boric acid, 44.5×10^{-3} M; EDTA, 1×10^{-3} M; pH = 8.0) at room temperature for 24 h. After the polypeptide absorption/conjugation onto the rGO, excess polypeptide was removed and the conjugated rGO was washed by centrifugation at 20 000 G three times. The recovered, conjugated rGO concentrate was resuspended in 200 µL of TBE buffer.

Assembly and Surface Modification of the QDs: The organic, soluble, core-shell CdSe/ZnS QDs were a gift from Oceannanotech LLC. They contained a surfactant coating (TOPO) on the surface. QD self-assembly was carried out using a microemulsion process. The core-shell CdSe/ZnS QDs (4 mg) were dispersed in chloroform and ultrasonicated for 3 min to form a homogeneous organic phase. A water phase was prepared by dissolving 20 mg of poly(vinyl alcohol) (PVA, $M_w \approx$ 9000–10 000 g mol^{-1}) as a polymer stabilizer to 1 mL of deionized (DI) water at 70 °C. The resulting clear solution was cooled to room temperature. Then, the organic phase was immediately added to the water phase, and the mixture was vigorously emulsified for several minutes using an ultrasonicator (Hielscher Ultrasound Technology, UP200S ultrasonic processor). The emulsion was next stirred at room temperature for 24 h to evaporate the organic solvent and form the self-assembled QD nanospheres, and the nanostructure was examined by TEM. To modify the initial hydrophobic surfactant (TOPO) on the QDs, 11-mercaptoundecanoic acid (MUA) or 3-mercaptopropionic acid (MPA) was used to replace the TOPO partially, according to a modified method of Breus and coworkers.[34] Briefly, the MUA or MPA (1.7×10^{-3} m mol) and the QDs (3.4×10^{-4} m mol) were dissolved in chloroform (20 mL). The mixture was then adjusted to pH = 12 with tetramethylammonium hydroxide pentahydrate (TMAHP). The flask was purged with N_2 and kept at room temperature for 24 h to cause TOPO/MUA substitution. The hydrophilic QDs were separated from the chloroform by adding ethanol to the solution. The ethanol solution of the QDs was washed and centrifuged at 10 000 rpm for 15 min 3 times. The final mixture was redissolved in water.

Assemblies of QD-rGO: To prepare the QD-rGO, poly(L-lysine)-rGO was mixed at different ratios with MUA-coated QDs in TBE buffer in the presence of 0.1 M NaCl. The QDs used had an emitting signal at about 600 nm in this system. Following incubation for 24 h at room temperature, the mixture became well dispersed in water, appeared in a transparent brown color, and was ready for examination by TEM.

Photothermal Irradiation and In Situ Optical Monitoring: After 18 h of incubation with the QD-rGO, the cell pellets were irradiated for 4 min in a 2 cm dish using an 808 nm laser at a power of 2 W cm^{-2} (0.25 cm^2 laser area). The source laser was a 20 W, 808 nm diode laser. After irradiation, the cells were stained with propidium iodide to characterize the cell viability (live ones showing green). The fluorescence images of the live cells and the QD-rGO were also observed using an inverted Nikon microscope and a confocal microscope.

Supporting Information

Supporting Information is available from the Wiley Online Library or from the author.

Acknowledgements

This work was financially supported by the National Science Council of the Republic of China, Taiwan under Contract of NSC 100-2320-B-009-006-MY2 and NSC 99-2221-E-009-070-MY3. This work is also supported by the "Aim for the Top University" program of the National Chiao Tung University and Ministry of Education, Taiwan, R.O.C. I.-W.C. acknowledges support from Army Medical Research & Material Command Grant No. W81XWH-10-1-0320 and W81XWH-10-1-0604. We are grateful to Prof. X. H. Gao. and the University of Washington for the quantum-dot analysis and fruitful discussion.

Received: October 24, 2011
Revised: December 28, 2012
Published online: March 16, 2012

[1] X. Michalet, F. F. Pinaud, L. A. Bentolila, J. M. Tsay, S. Doose, J. J. Li, G. Sundaresan, A. M. Wu, S. S. Gambhir, S. Weiss, *Science* **2005**, *307*, 538.
[2] J. A. Barreto, W. O'Malley, M. Kubeil, B. Graham, H. Stephan, L. Spiccia, *Adv. Mater.* **2006**, *23*, H18.
[3] Z. Ge, J. Hu, F. Huang, S. Liu, *Angew. Chem. Int. Ed.* **2009**, *48*, 1798.
[4] Z. Hu, X. Xia, *Adv. Mater.* **2004**, *16*, 305.
[5] X. Z. Zhang, D. Q. Wu, C. C. Chu, *Biomaterials* **2004**, *25*, 3793.
[6] M. Krämer, J. F. Stumé, H. Türk, S. Krause, A. Komp, L. Delineau, S. Prokhorova, H. Kautz, R. Haag, *Angew. Chem. Int. Ed.* **2002**, *41*, 4252.

[7] I. L. Medintz, H. T. Uyeda, E. R. Goldman, H. Mattoussi, *Nat. Mater.* **2005**, *4*, 435.
[8] N. Lewinski, V. Colvin, R. Drezek, *Small* **2008**, *4*, 26.
[9] R. Generalov, S. Lukoseviciute, A. Juzeniene, P. Juzenas, *IEEE J. Selected Topics Quantum Electron.* **2010**, *16*, 997.
[10] S. Lal, S. E. Clare, N. J. Halas, *Acc. Chem. Res.* **2008**, *41*, 1842.
[11] W. S. Kuo, C. N. Chang, Y. T. Chang, M. H. Yang, Y. H. Chien, S. J. Chen, C. S. Yeh, *Angew. Chem. Int. Ed.* **2010**, *49*, 2711.
[12] H. K. Moon, S. H. Lee, H. C. Choi, *ACS Nano* **2011**, *3*, 3707.
[13] J. T. Robinson, S. M. Tabakman, Y. Liang, H. Wang, H. S. Casalongue, D. Vinh, H. Dai, *J. Am. Chem. Soc.* **2011**, *133*, 6825.
[14] Z. Liu, J. T. Robinson, X. Sun, H. Dai, *J. Am. Chem. Soc.* **2008**, *130*, 10876.
[15] K. Yang, S. Zhang, G. Zhang, X. Sun, S. T. Lee, Z. Liu, *Nano Lett.* **2010**, *10*, 3318.
[16] X. Sun, Z. Liu, K. Welsher, J. T. Robinson, A. Goodwin, S. Zaric, H. Dai, *Nano Res.* **2008**, *1*, 203.
[17] X. Yang, Y. Wang, X. Huang, Y. Ma, Y. Huang, R. Yang, H. Duan, Y. Chen, *J. Mater. Chem.* **2011**, *21*, 3448.
[18] H. Dong, W. Gao, F. Yan, H. Ji, H. Ju, *Anal. Chem.* **2010**, *82*, 5511.
[19] B. Farrow, P. V. Kamat, *J. Am. Chem. Soc.* **2009**, *131*, 11124.
[20] N. Nakayama-Ratchford, S. Bangsaruntip, X. Sun, K. Welsher, H. Dai, *J. Am. Chem. Soc.* **2007**, *129*, 2448.
[21] W. S. Hummers, R. E. Offeman, *J. Am. Chem. Soc.* **1958**, *80*, 1339.
[22] J. Zhuang, H. Wu, Y. Yang, Y. C. Cao, *Angew. Chem. Int. Ed.* **2008**, *47*, 2208.
[23] J. Zhuang, H. Wu, Y. Yang, Y. C. Cao, *J. Am. Chem. Soc.* **2007**, *129*, 14166.
[24] D. Wang, T. Xie, Q. Peng, Y. Li, *J. Am. Chem. Soc.* **2008**, *130*, 4016.
[25] V. Hlady, J. Buijs, *Curr. Opin. Biotechnol.* **1996**, *7*, 72.
[26] J. Liu, S. Fu, B. Yuan, Y. Li, Z. Deng, *J. Am. Chem. Soc.* **2010**, *132*, 7279.
[27] J. Yu, T. Ma, S. Liu, *Phys. Chem. Chem. Phys.* **2011**, *13*, 3491.
[28] M. Han, X. Gao, J. Z. Su, S. Nie, *Nat. Biotechnol.* **2001**, *29*, 631.
[29] H. Choi, S. R. Choi, R. Zhou, H. F. Kung, I.-W. Chen, *Academic Radiology* **2004**, *11*, 996.
[30] P. S. Low, W. A. Henne, D. D. Doorneweerd, *Acc. Chem. Res.* **2008**, *41*, 120.
[31] O. C. Farokhzad, R. Langer, *ACS Nano* **2009**, *3*, 16.
[32] J. Huang, L. Bu, J. Xie, K. Chen, Z. Cheng, X. Li, X. Chen, *ACS Nano* **2010**, *4*, 7151.
[33] D. I. Lubyshev, P. P. González-Borrero, E. Marega Jr., E. Petitprez, N. La Scala Jr., P. Basmaji, *Appl. Phys. Lett.* **1996**, *68*, 205.
[34] V. V. Breus, C. D. Heyes, G. U. Nienhaus, *J. Phys. Chem. C* **2007**, *111*, 18589.